ACCEPTED VERSION

Peipei Jia, Kamil Zuber, Qiuquan Guo, Brant C. Gibson, Jun Yang and Heike Ebendorff-Heidepriem

Large-area freestanding gold nanomembranes with nanoholes

Materials Horizons, 2019; 5(5):1005-1012

Published at: http://dx.doi.org/10.1039/C8MH01302K

Materials Horizons

Accepted Manuscript

This article can be cited before page numbers have been issued, to do this please use: P. Jia, K. Zuber, Q. Guo, B. C. Gibson, J. Yang and H. Ebendorff-Heidepriem, *Mater. Horiz.*, 2019, DOI: 10.1039/C8MH01302K.

ROYAL SOCIETY OF CHEMISTRY

rsc.li/materials-horizons

View Article Online
DOI: 10.1039/C8MH01302K

Conceptual Insights

In this article, we present a new generation of wafer-scale freestanding gold nanomembranes (NMs) penetrated with nanohole arrays. These NMs are made by a simple, scalable, high-throughput replication-releasing procedure, which has the potential to be extended to other compatible materials. Such freestanding NMs allow us to explore their inherent properties without substrate effects for the first time. With an extremely narrow plasmonic resonance, they achieve an excellent figure-of-merit when used as ultrathin surface plasmon resonance (SPR) sensors, far exceeding the previous record of their kind on substrate and the theoretical limit for standard prism-based gold SPR sensors. The presence of nanoholes can dramatically decrease the in-plane modulus of freestanding gold NMs. In comparison with thickness variation, structural engineering is a more effective way to modulate mechanical properties of these thin membranes. The freestanding gold NMs can be geometrically convert to 3D microstructures using a low dose ion-irradiation-based kirigami technique. This provides a route to realize complex microsystems and their conformation manipulation. In addition, our freestanding gold NMs can be attached to various otherwise impossible substrates, making them more attractive for potential hetero-integration with advanced optical and electronic systems for new applications.

Large-area Freestanding Gold Nanomembranes with Nanoholes

DOI: 10.1039/C8MH01302K

Peipei Jia[1,2,3], Kamil Zuber[4], Qiuquan Guo[3,5], Brant C. Gibson[1,6], Jun Yang[5] and Heike Ebendorff-Heidepriem[1,2,*]

[1]ARC Centre of Excellence for Nanoscale BioPhotonics (CNBP)

[2]Institute for Photonics and Advanced Sensing (IPAS), School of Physical Sciences, The University of Adelaide, Adelaide, SA 5005 Australia

[3]Shenzhen Topmembrane Technology Co., Ltd., Shenzhen, Guangdong 518000 China

[4]Future Industries Institute, University of South Australia, Mawson Lakes, SA, 5095 Australia

[5]Department of Mechanical & Materials Engineering, Western University, London, Ontario N6A 3K7 Canada

[6]School of Science, RMIT University, Melbourne, VIC 3001 Australia

* heike.ebendorff@adelaide.edu.au

ABSTRACT

Thin metal films with nanohole arrays have opened up new opportunities in applications ranging from plasmonics to optoelectronics. However, their dependence on substrates limits not only their performance but also other application possibilities. A key challenge to overcome this limitation is to make these nanostructured films substrate-free. Here we report large-area freestanding gold nanomembranes with nanohole arrays fabricated using a replication-releasing procedure. The structures maintain spatial uniformity and pristine quality after release across the entire membrane up to 75 cm^2 in area and as thin as 50 nm. The freestanding nanomembranes show significantly enhanced optical transmission and effective field extension compared to the same nanomembranes on substrates. A plasmonic coupling resonance with a 2.7 nm linewidth achieves a record figure-of-merit of 240 for refractive index sensing. The gold nanomembranes can be geometrically converted to 3D microstructures by ion-irradiation-based kirigami technique. The transformed micro-objects can be precisely controlled via geometry design and strategic cutting. Furthermore, we find the presence of nanoholes can significantly change the in-plane modulus of the gold nanomembranes. Finally, the freestanding gold nanomembranes can be transferred to non-planar substrates, enabling their future integration with advanced optical and electronic systems for emerging applications.

Introduction

Nanomembranes (NMs) are functional materials with nanoscale thicknesses and macroscopic lateral dimensions. They possess many unique electronic, mechanical and optical properties, not found in zero- and one-dimensional materials[1]. Freestanding NMs have been made of inorganic matter (e.g. silicon, graphene, polymer) [2-7], organic materials (e.g. resin)[8] and hybrid composite[9-11]. Among metals, gold is particularly suited as NM material as it can be laminated into around 100-nm-thin unbroken sheets. Recent research revealed thin gold films possess mechanical properties different from the bulk.[12] Many other metal NMs with novel properties are assembled from their building blocks of nanoparticles[10, 13, 14] or nanowires[15] on solution interfaces. For example, a new electron

View Article Online
DOI: 10.1039/C8MH01302K

transport regime was disclosed in a gold nanoparticle suspended NM.[16] These NMs are freestanding, yet not perforated. In contrast, regular arrays of nanoholes have been patterned into noble metal films on planar substrates, [17] holding great potential for the next generation of plasmonic sensors, colour filters and planar nanolens.

In general, it is desirable to have high quality factor plasmonic resonances and enhanced near-fields for strong light-matter interactions for these devices. However, because perforated metal films are usually fabricated on planar substrates, their transmission efficiency suffers from the different dielectric environment on either side.[18] Moreover, the on-substrate configuration also limits the possibility of exploring their mechanical properties and further potential applications. Although substrate manipulation [18] [19] is an effective route to reduce this substrate effect, the freestanding NMs could possess completely identical dielectric surroundings and thus optimal resonances. However, challenges arise from fabricating large-area metal NMs with both freestanding modality and nanohole arrays at the same time. Previous efforts have realized such combination with advanced fabrication methods for nanohole generation,[20-23] followed by separation of NMs from substrates. However, the released NMs have either small lateral size (typically in mm ranges), random hole arrangement or have been finally transferred to substrates without further freestanding investigation. Another modality is a quasi-freestanding metal membrane on a suspended SiN layer (< 200 nm) with nanohole arrays through both layers.[24-26] These nanohole arrays have been used as plasmonic sensors that have achieved the highest performance of their kind.

Here, we report the generation of large-area freestanding gold NMs perforated with nanohole arrays using a template transfer technique. Gold NMs can sustain wafer-scale integrity and uniformity of through nanoholes. Such freestanding NMs allow us to explore their inherent functional properties without substrate effects. The 100 nm gold NMs show significant transmission enhancement and effective extension of electromagnetic field compared to the same structures on glass substrates. More importantly, an extremely narrow resonance is observed and achieves a record high sensing performance when the freestanding membranes are used as plasmonic refractometric sensors. By ion irradiation, freestanding NMs can be converted from 2D layouts to 3D structures. Various configurations can be precisely transformed, showing great design flexibility on geometry and conformation. We find that the mechanical properties of gold NMs are dramatically altered due to the presence of nanoholes. Finally, we also show the gold NMs can be attached to various non-planar substrates. Such integration is promising to lead to new functional devices and a wide range of novel applications.

Results and Discussion

Fabrication

The schematic in Figure 1(a) depicts the fabrication process of wafer-scale freestanding gold NMs with nanohole arrays. Our method is based on the template transfer technique that uses a pre-patterned Si wafer (Eulitha AG) with nanoholes (diameter tolerance +/-10%, array period tolerance +/-1nm, 350 nm depth, and defect area less than 1%) as the template to form gold membranes with similar geometry and thus physical properties. To enable the release of the gold NM, 50 nm copper as a sacrificial layer is first deposited onto the template followed by gold deposition (50 nm to 100 nm) either using thermal or electron-beam evaporation. These physical vapour depositions are

highly anisotropic, e.g. only in the vertical direction, where the metal does not adhere to the side walls of the Si nanoholes. On condition that the depth of the Si nanoholes is larger than the total thickness of copper and gold, this deposition technique ensures the disconnection between the deposited membrane on top of the patterned Si wafer and the deposited nanodisks in the holes. Thus nanohole arrays are naturally replicated during gold deposition. To release the NM from the template, the Si template is settled obliquely in a container, where $FeCl_3$ solution as a copper etchant is slowly poured in at the beginning to initiate the etching. As the solution level rises, the contact line starts splitting the gold NM from the template, and surface tension from the etchant keeps the released part of the NM floating flatly on the solution surface. The oblique setup enables slow release as the NM is gradually exposed to the etchant during etching (Figure S1, Supporting Information). To ensure a smooth release, the rising speed of the etchant can always been adjusted according to the oblique angle of the template to match the copper etching rate. The releasing setup for our NMs is quite flexible and robust. We have seen no quality difference in our gold NMs released with various speeds. This large-area and low-cost replication-releasing method is particularly suitable for batch production because the template can be re-used after cleaning. In addition, it has the potential to extend to other materials that could be deposited on a template assuming compatible sacrificial layer and etchant.

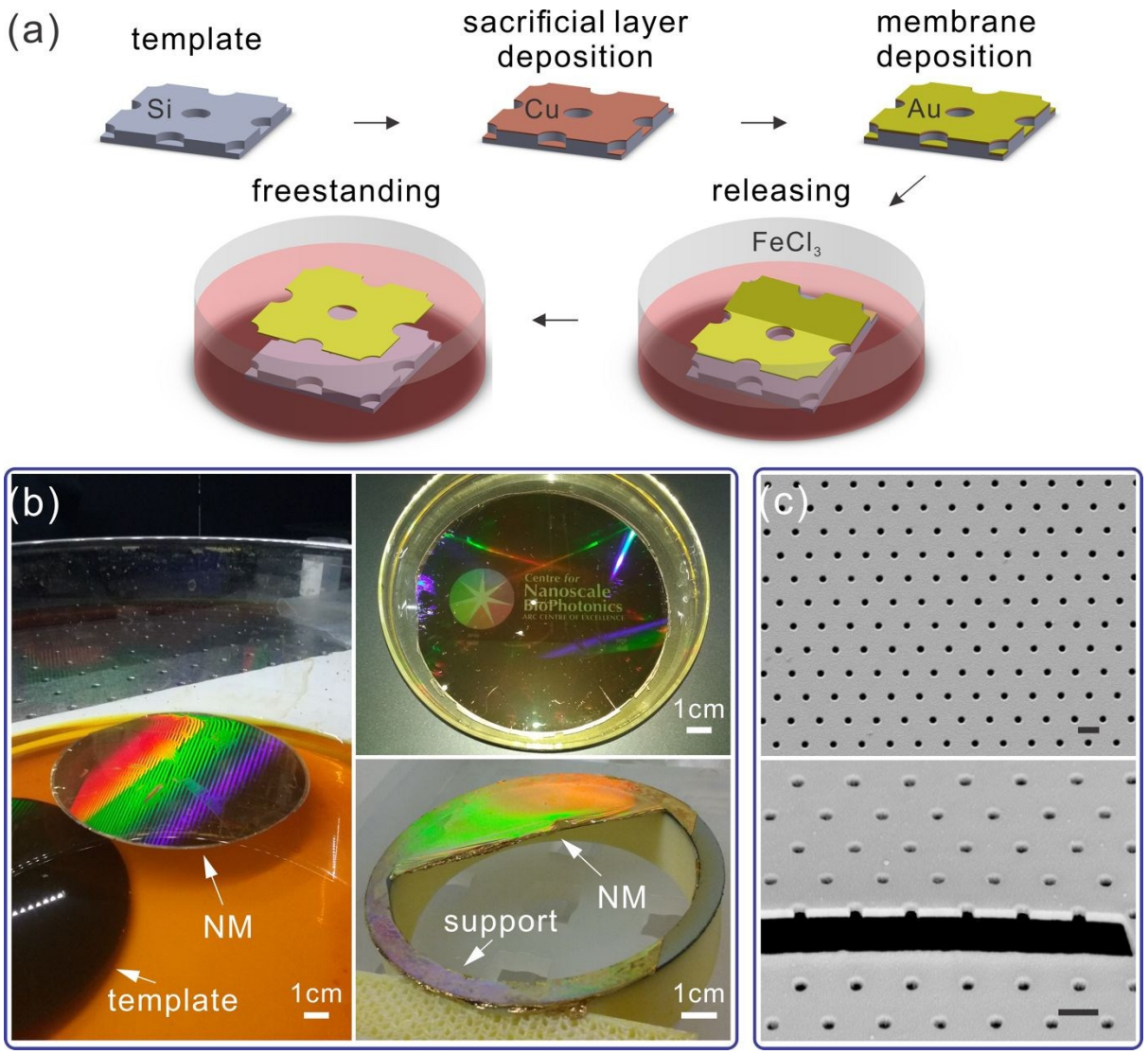

View Article Online
DOI: 10.1039/C8MH01302K

Figure 1. (a) Schematic of fabrication process of freestanding gold nanomembranes (NMs): pre-patterned Si template; copper deposition; gold NM deposition; etching and releasing; freestanding NM floating on solution surface. (b) Left: a pristine 10 cm gold NM floating on the etchant surface after released from the template; Top-right: a partially transparent ultrathin (50 nm) gold NM on water in a glass petri dish with a logo underneath the petri dish; Bottom-right: a 100 nm gold NM suspended across a support in free space. (c) Scanning electron microscope images of a NM showing an array of penetrating holes (diameter, *D*=200 nm; period, *P*=700 nm) in the top image and a focused ion beam milled region in the bottom image where the thickness of the membrane can be observed. Scale bars, 500 nm.

Figure 1b (left) highlights a 50-nm-thin freestanding gold NM after complete release from the template. It has an area of 75 cm^2, with a hexagonal array of around 2.5×10^{10} nanoholes (*D*=250 nm, *P*=600 nm). Strong diffraction can be observed from this nanohole array. Despite being made of gold, this ultrathin membrane becomes partially transparent due to the presence of nanoholes, by which the logo on the other side is visible (Figure 1b, top-right). A metal film with less than 100 nm thickness is very fragile, and the presence of high-dense nanoholes makes it even more delicate. However, large-area 100-nm-thin gold membranes can still be freed from the aqueous solution (Figure 1b, bottom-right; fabrication process detailed in Figure S2, Supporting Information). Although broken, the remaining NM of more than 5 cm^2 still far exceeds the size of previous reported freestanding gold nanohole arrays in the air. This enables applications that require dry freestanding membranes. As shown in the top image in Figure 1c, the freestanding NMs have a smooth surface and the same well-ordered pattern as that of the template. Its cross-section, shown in the bottom image in Figure 1c, reveals the nanoholes are open on both sides. These images confirm high structure fidelity is achieved in our freestanding NMs.

Plasmonic properties

The plasmonic resonances and field enhancement of the NMs are investigated through transmission measurements. We compare the transmission spectra (Figure 2a) of two identical 100-nm-thin perforated NMs (*D*=200 nm, *P*=700 nm) replicated from the same template: one freestanding in air (shown in Figure 1c) and the other placed on a glass substrate (refractive index 1.52). The transmission of a 100-nm-thin freestanding gold NM without nanoholes is also recorded for reference. All the spectra have a peak at 500 nm from direct transmission of light through the gold film owing to the band transition of gold.[27] Transmission efficiency on resonance for the freestanding NM at 700 nm is tripled compared to the NM on substrate.

To understand the physics behind these spectral features, we performed simulations using finite-difference time-domain (FDTD) method. Excellent agreement with experiment is achieved for the transmission spectra. On substrate, the different dielectric materials (air and glass) on either side of the nanohole array results in multiple resonant peaks at different wavelengths, e.g. 700 nm and 1000 nm. In contrast, the same dielectric condition in the vicinity of the freestanding NM matches the surface plasmon energy on both surfaces, resulting in a coupling resonance and consequently remarkable transmission enhancement at the resonance at 700 nm.[18] The peak at 580 nm is attributed to a high-order mode resonance. The simulations show the electric field at the resonance is a symmetric coupling mode in the freestanding case (inset in Figure 2b). Note that the measured

View Article Online
DOI: 10.1039/C8MH01302K

transmission peaks are broader than those in simulation. This is possibly due to nonradiative loss caused by material absorption of gold and surface roughness.

The electromagnetic field distribution is critical for near-field applications such as biosensing and surface-enhanced Raman spectroscopy (SERS).[28] Because of the higher refractive index of substrates such as glass and quartz compared to air or buffer solutions, the enhanced field is mainly located inside the substrate (Figure 2b, inset). Such field distribution of on-substrate nanohole array NMs deteriorates these sensors' performance because the field in the substrate is inaccessible to external analytes. Changing substrate geometry can partially relieve this issue. For example, gold-SiN bilayer membranes have achieved highly sensitive and narrow plasmonic resonances owing to being quasi-freestanding.[24] In contrast, the entire field around our freestanding NMs extends into free space and thus is fully accessible to the analyte.

In the sensitivity measurement using aqueous solutions with different refractive index, two coupling plasmonic resonances (bright at 925 nm and dark at 865 nm, Figure 2c) are observed. The bright mode is due to symmetric coupling between the resonances of both surfaces, whereas the dark mode is owing to asymmetric coupling as shown in E-field vector mapping (Figure 2d). The refractive index sensitivity (defined by the slope of resonance wavelength as a function of the surrounding refractive index n) as high as 650 nm/RIU is obtained in water for both resonances. This sensitivity approaches the theoretical limit in this wavelength range for these types of nanostructure arrays.[29] The simulation also confirms this result with 655 nm/RIU and 648 nm/RIU for dark and bright mode, respectively. Remarkably, the dark-mode resonance reaches an extreme narrow linewidth (the full width at half maximum, $FWHM$ = 2.7 nm). This is attributed to the quadrupole nature of the coupling mode, resulting in a suppression of radiative damping and thus a prolonged resonance lifetime. The corresponding figure of merit (FOM=sensitivity/linewidth, a widely accepted performance indicator for plasmonic sensors) of 240 far exceeds the previous record value of 162 for nanohole arrays and the theoretical limit of 108 for standard prism-based gold plasmonic sensors.[24]

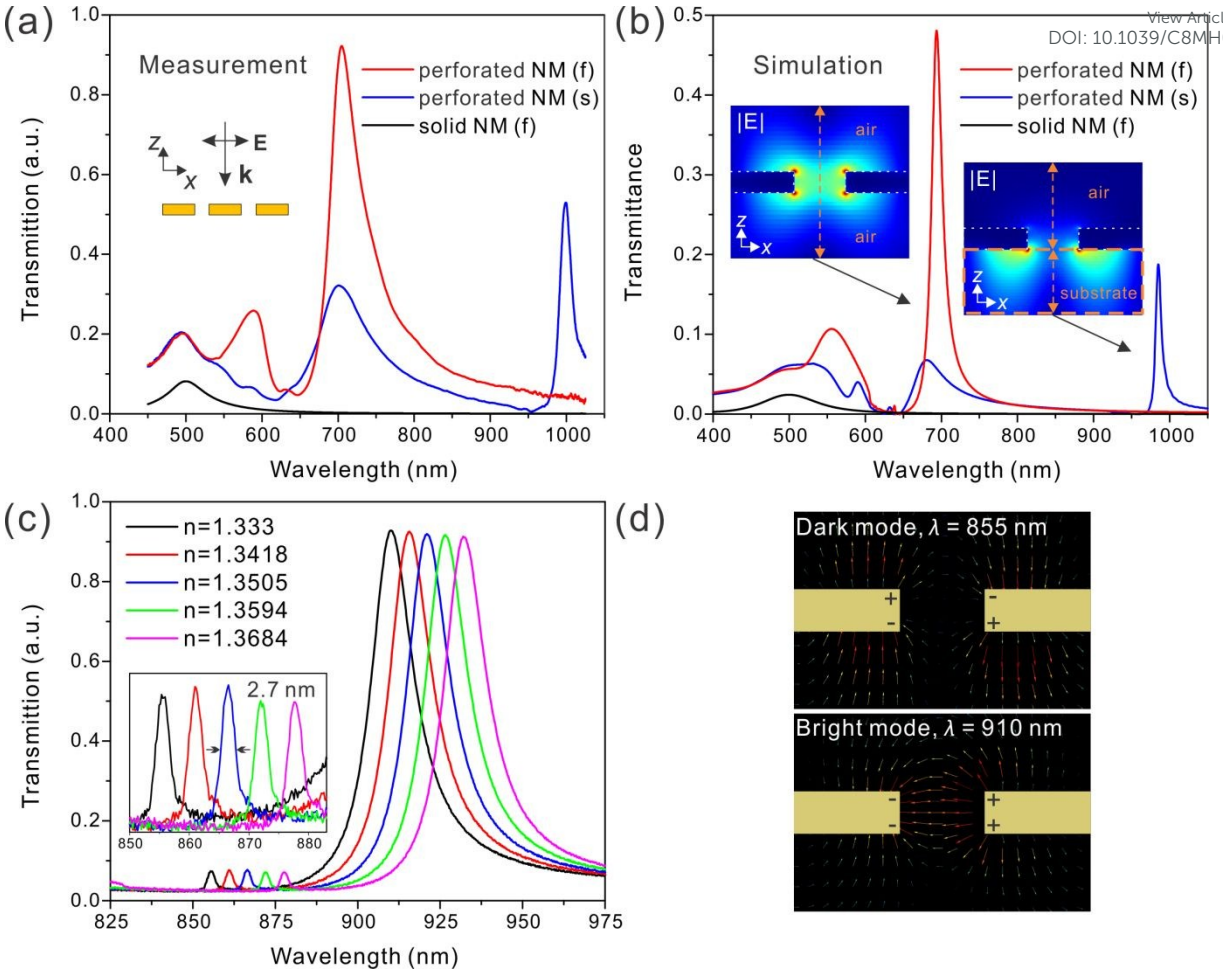

Figure 2. Plasmonic properties of freestanding gold NMs. (a) Measured and (b) simulated transmission of 100-nm-thin NMs: freestanding nanohole array NM [perforated NM (f), red], on-substrate nanohole array NM [perforated NM (s), blue] and freestanding solid NM without nanoholes [solid NM (f), black]. Insets in (b): Simulated electric field distributions for strongest resonance in *x-z* cross-section (x is polarization direction along one translation axis of the nanohole array, and *z* is out-of-plane direction) of the nanoholes in freestanding and on-substrate NMs. Both field mappings have the same scale. The dash lines indicate the cross-sections of NMs and the substrate. (c) Sensitivity measurement in aqueous solutions with various refractive indexes. Inset: Peaks between 850 nm to 880 nm are related to a narrow dark-mode coupling resonance. Note that dark mode is the small features around 635 nm in (a) and (b). (d) Simulated electric field vector mapping on the dark and bright resonances reveal different coupling modes.

3D structure transformation

Controllable transformation of NMs to 3D structures is of importance for the construction of functional devices at the microscale. One research interest is to realize such change by introducing 'cuts and folds' with the kirigami technique.[30] For thin films, one suitable method is the use of a focused ion beam (FIB) for both cutting and bending. [31-34] Our approach includes two steps: cutting the NMs into the desirable suspended components by ion milling and then folding them by scanning their surfaces in FIB imaging mode. Compressive stresses induced by ion irradiation can deform the suspended NMs into engineered 3D configurations.[35] For our ultrathin gold NMs, using high-dose

View Article Online
DOI: 10.1039/C8MH01302K

ions causes serious damage to their nanoholes and uncontrolled transformation process (Figure S3, Supporting Information). Therefore, low-dose ions (1.5 pA and ~2×10^3 ions/μm^2/scan, respectively) are used to mill and irradiate the NMs. Recently, the high-dose milling and low-dose global irradiation were combined to realize solid-film gold nanostructures for nanophotonic applications.[36] The total dose in the range of ~10^6 to 10^7 ions/ μm^2 was used in their surface irradiation, compared to <10^5 ions/ μm^2 in our technique. It is noted some of those gold surfaces and small structures were notably damaged after irradiation.

The bending angles as a function of ion dose are measured for 100-nm-thin gold NMs with constant nanohole diameter (D=250nm) for various period of the nanohole array (resulting in different air filling fractions defined as D/P), and various area and aspect ratio of the cut section (defined as $aP\times bP$ and a/b, respectively, where aP and bP are the lateral dimensions of a cut section as shown in Figures 3a and b). For similar area of the cut section (Figure 3a, a=3 or 5 and b=1 or 3, corresponding to areas 1-3 μm^2), the suspended, cut sections with higher aspect ratio of a/b=3 and 5 are easier to be bent up compared with a/b=1. For similar aspect ratio of the cut section (Figure 3a, a/b in the range of 1-3), larger area of the cut section (a=10 and b=5, corresponding to area of 18 μm^2) results in smaller bending angle. Increasing air-filling fraction due to smaller period of nanohole arrays for the same hole-diameter (D/P=0.36, 0.42 and 0.50 in Figure 3b) likely allows more ions to go through the holes rather than onto the NM surfaces. However, this led only to a small decrease in the bending angle. One benefit of surface scanning is simultaneously bending multiple objects in one snapshot (Figure 3c). As being monitored via *in situ* SEM, the assembly can instantly be ceased at any moment by blocking ion irradiation, enabling a real-time process control.

Previous 3D transformation of NMs was limited to regular or symmetric objects. Here we also realize controlled asymmetry transformation via deliberate design of cutting patterns and geometries. First of all, cutting sequences must be selected carefully to keep irregular objects in balance after shaping (Figure S4, Supporting Information). Otherwise, the object may not have a proper initial attitude. Secondly, bend behaviour is programmed by choice of geometries, which determine the stress distribution during irradiation. For example, besides compressive forces, in-plane torques can be simultaneously induced during ion irradiation via strategic shaping the wings of the butterfly (Figure 3d). Remarkably, the tips of two front wings touch each other after travelling a curved trajectory (Figure S3, Supporting Information). Occasionally, it is desired to lift some parts while keeping others unchanged. In Figure 3e, when the legs are all lifted up via ion exposure, the disk keeps almost in the same position due to its symmetric bonds to the legs. These examples show FIB-based kirigami is a suitable technique to provide opportunities for further development of NMs. We envisage the NM kirigami will have many potential applications in special scenarios that require small gears in the areas of optomechanics and 3D optics.

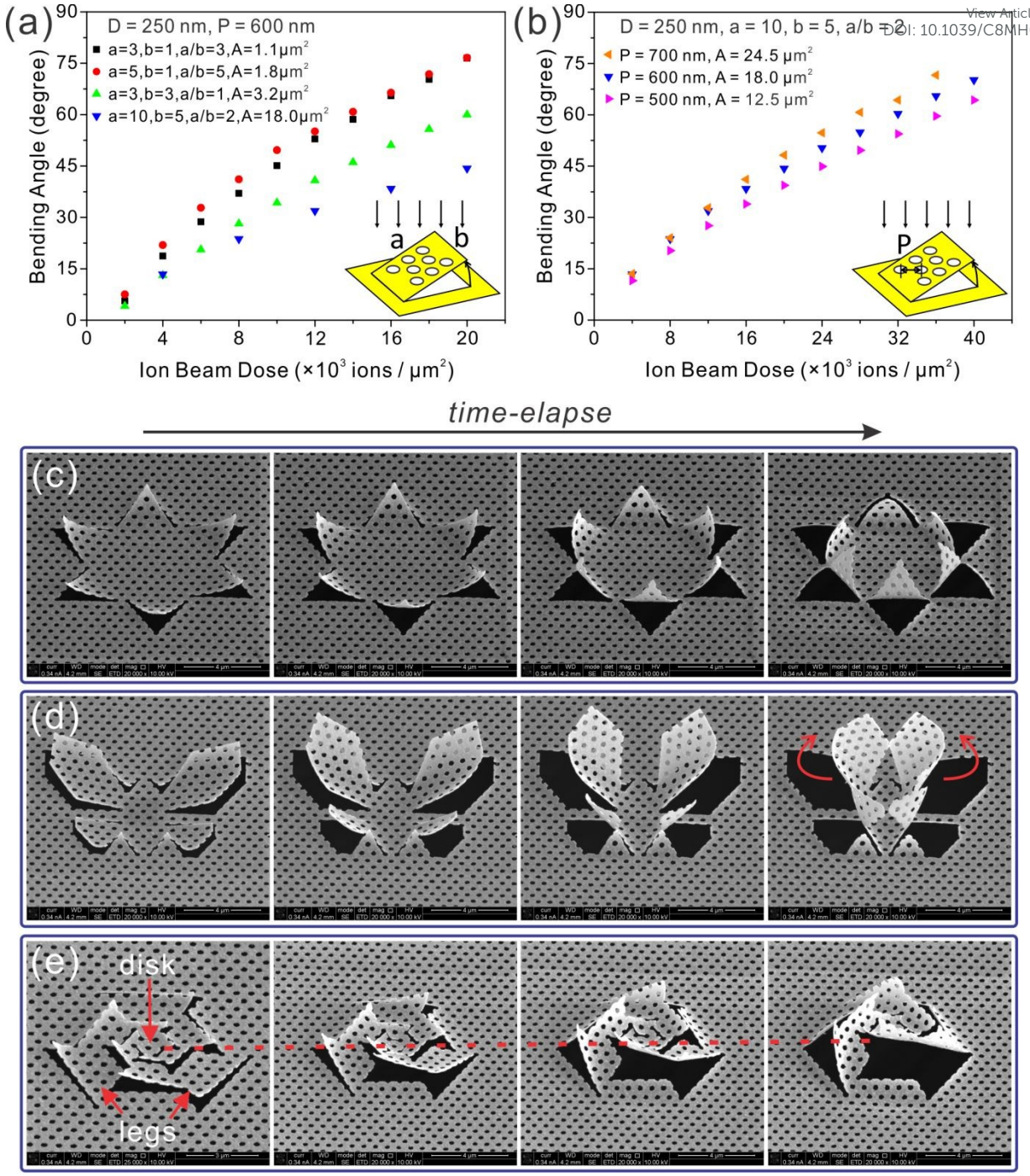

Figure 3. 3D transformation by ion beam cutting and irradiation for 100-nm-thin nanohole array gold NMs (D = 250 nm). Bending angles of suspended, rectangular cut sections measured as a function of ion beam dose: (a) different cut section area ($aP \times bP$, P = 600nm) and different aspect ratio (a/b), (b) different nanohole periods at constant cut section lateral dimensions (a=10, b=5). Transformation dynamics by programmable cutting and surface ion scanning. The time-elapse SEM images show: (c) simutinuously bending of all the petals, (d) twisting of the butterfly wings, and (e) suspending of the spring's central disk.

Mechanical properties

View Article Online
DOI: 10.1039/C8MH01302K

To determine the mechanical strength of our freestanding gold NMs, we performed atomic force microscopy (AFM) indentation. The in-plane modulus is evaluated by collecting force curves measured via deflecting the 100-nm-thin gold NM placed over transmission electron microscopy (TEM) grid. All the samples are made using the same deposition process to exclude the possibility that the modulus difference is due to difference fabrication conditions. The slope of the force curves (Figure 4a) is determined by performing linear fitting on the measured force curves in the contact zone. The calculated in-plane modulus is 705 ± 39 GPa for the solid gold NM without holes and 202 ± 23 GPa for the perforated NM (D = 250 nm, P = 600 nm) of the same thickness (detailed calculation in Supporting Information). The results show a close to four-fold modulus change induced by the presence of nanoholes. Previous studies showed mechanical properties of thin metal films can be tuned by thickness variation, however, in a relative narrow range (~20%).[12, 37] Alternatively, our NMs offers structural engineering as a more effective way of tuning mechanical properties of thin membranes.

Transfer to non-planar substrates

Previously, transfer printing has enabled the integration of thin membranes on the planar/outer surface of targets.[38] However the deployment on inner surfaces and highly curved surfaces is still challenging. As our gold NMs are freestanding, we have more freedom in transferring them not only to planar substrates, but also to virtually any support of arbitrary geometry. To show this merit, we deploy them onto a diverse range of substrates. Notably, the gold NMs on curved surfaces (e.g. the apple in Figure 4b) can retain its diffraction pattern, which indicates that the nanohole array maintains its structure after transfer. By transferring a gold NM onto the inner surface of a glass vial (Figure 4b), we show the potential of their deployment in inaccessible locations. Gold NMs can also be wrapped around optical fibers (Figure 4c). Due to its 50 nm thickness and flexibility, the NM can conformably adhere to the curved fiber surface without cracking.

Beyond on-substrate use, some applications may demand nanoholes unblocked on both sides of the gold NM. For example, single-particle electron cryomicroscopy (cryoEM) requires thin films with penetrating holes to hold proteins for transmission imaging. Previous work demonstrated a 50 nm gold foil with micron-size holes on a TEM grid eliminates substrate motion during irradiation for better resolution .[39] Sample supports with smaller holes tend to reduce this beam-induced motion.[40] Thus, our gold NMs with nanoholes, which can also cover TEM grids (Figure 4d), have the potential to work as specimen supports to further inhibit sample motion for single particle cryoEM imaging.

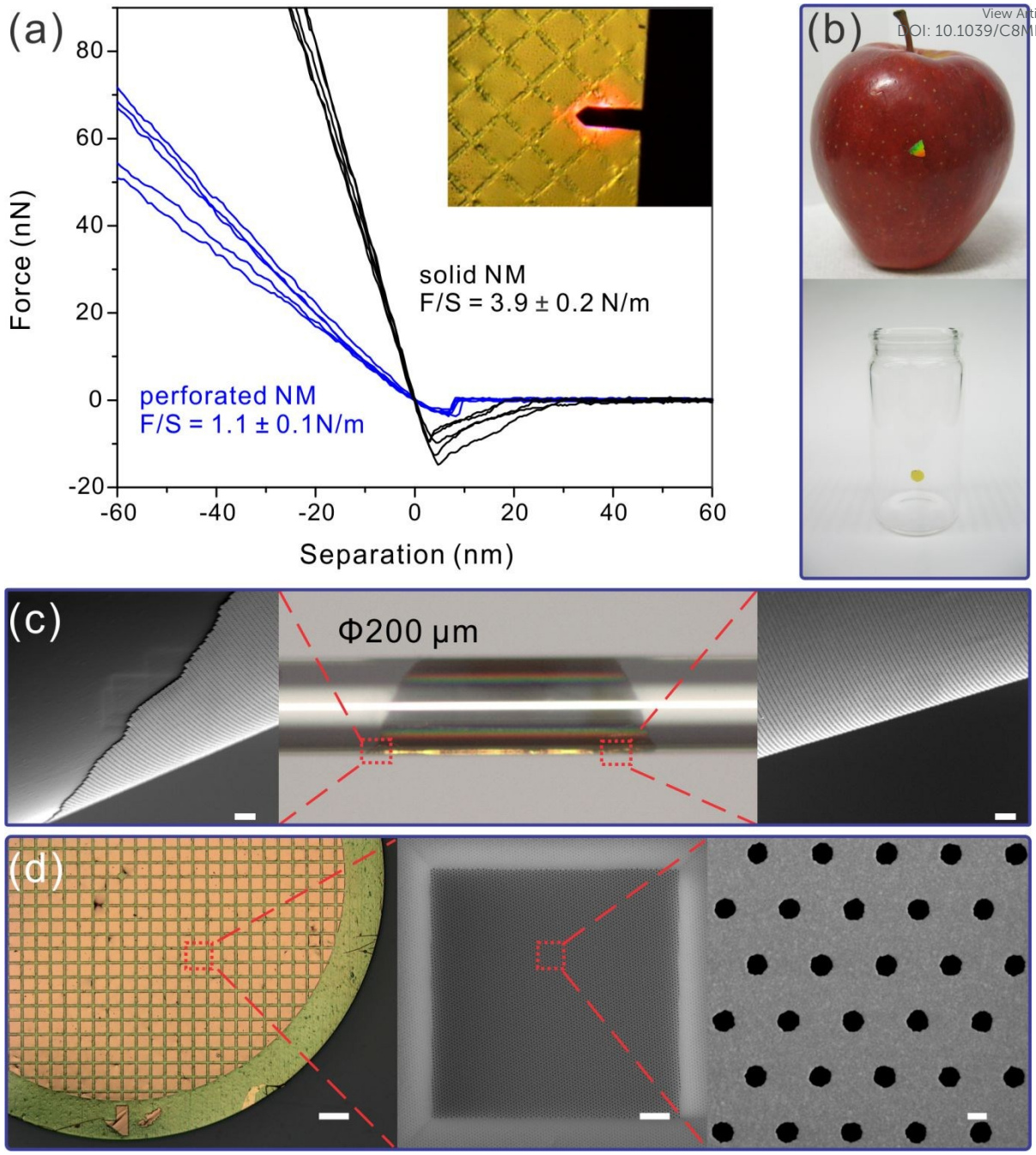

Figure 4. Mechanical properties and transfer of freestanding NMs. (a) AFM force curves for in-plane modulus calculations on both solid (black curves) and perforated NMs (blue curves). F/S is the absolute value of the slope of the force curves (F, the applied force; S, the separation between NM and the AFM tip). Inset: top view camera image of the measured sample showing the AFM tip and laser. Attachment of NMs on unusual substrates: (b) Rough surface of an apple (top) and inside wall of a glass vial (bottom), (c) Optical fiber (the optical image in the middle with two zoom-in SEM images. Scale bars, 2 μm) and (d) TEM grid (Scale bars, 100 μm, 10 μm, 200 nm for the left optical image and right, two SEM images respectively). Thicknesses of NMs and periods of nanohole arrays are 100 nm and 700 nm for those in (b), and 50 nm and 600 nm for those in (c) and (d), respectively.

Summary and Conclusions

View Article Online
DOI: 10.1039/C8MH01302K

In summary, we present a simple yet efficient technique to fabricate wafer-scale freestanding gold NMs with regular arrays of nanoholes. Our replication-releasing method can be directly applied to any other material that can be deposited on pre-patterned templates. As these freestanding NMs are fragile, a practical way of large-area preservation is to attach them on some substrates (e.g. water soluble polymers) that could be easily dissolved before their use. Due to the dielectrically matched surroundings on either side, freestanding gold NMs show a 3-fold enhanced optical transmission and significant electromagnetic field extension compared to those on substrates. In particular, a highly sensitive dark-mode coupling resonance achieves a record FOM of 240 in refractive index sensing. Moreover, 2D freestanding NMs can be transformed into 3D structures using ion-beam kirigami technique. The combination of strategic cutting and in-situ folding using low ion dose enables advanced 3D transformation with unprecedented spatial and temporal flexibility. The freestanding modality also provides structure engineering as a way of mechanical property modulation for thin membranes. Finally, the freestanding gold NMs can be transferred onto a wide range of substrates, including inner and extremely curved surfaces, making them more attractive for potential hetero-integration and applications in plasmonic sensing, cryoEM and flexible electronics.

Experimental methods

Sensitivity measurement: Gold NMs were released and suspended across a 2mm single hole on a gold TEM grid (Agar Scientific). Then the grid was mounted in a grid holder (Microscopy Solutions) that allowed access to the NM from both sides. Two optical fibers were deployed near the surfaces of the NMs for transmission measurement. One optical fiber was used to deliver incident light from a white light source (HL-2000, Ocean Optics) to the gold NM and the other fiber was employed to collect transmission signals to a spectrometer (QE Pro, Ocean Optics). Refractive index solutions were prepared by adding NaCl into deionized water to obtain various concentrations (5%, 10%, 15% and 20%) with different refractive index. NaCl solutions were dropped onto one side of the NMs and flowed to the other side through the nanoholes. Transmission spectra were recorded until the solution completely covered the NM surfaces and touched the optical fiber tips.

FDTD simulation: 3D FDTD simulations were performed using a commercial software, FDTD Solutions (Lumerical Inc.). A uniform mesh size of 2 nm (x, y and z directions) was used. We set perfectly matched layer boundary conditions for the z direction, and periodic boundary conditions for x and y directions of the simulation region. The background indexes for freestanding NMs were set 1 or those of the NaCl solutions.

3D transformation: NM cutting and bending were done with a FIB/SEM dual beam microscope system (FEI Helios Nanolab 600). The FIB used 30 keV acceleration voltage, 1.5 pA ion current, 24 nm beam diameter and 50 ns dwell time. The folding process were monitored by in situ SEM during ion beam irradiation by snapshot in FIB imaging mode. All SEM images of the nanostructures were obtained immediately after operation.

In-plane modulus measurement: AFM measurements were performed using a Bruker Nanoscope V Multimode 8 AFM, using Tap 300 Al-G tips (BudgetSensors). The samples of 100-nm-thin gold perforated NM and solid NM were placed over TEM grids (G300, 300 Mesh Gold from SPI). The spring constant of the tip was calculated using thermal resonance spectra of the cantilever with the value being 15.6 N/m at the resonant frequency of 293 kHz. Prior to the test the measured area was

View Article Online
DOI: 10.1039/C8MH01302K

inspected by optical microscope to avoid measurements on buckled film. Each sample was tested at 6 different spots in the centre of the grid mesh.

Acknowledgments: This research is supported by the ARC Centre of Excellence for Nanoscale BioPhotonics (CNBP). This work was performed in part at Adelaide Microscopy, the South Australian node and Optofab node of the Australian National Fabrication Facility (ANFF) utilizing Commonwealth and SA State Government funding.

Reference

[1] J. A. Rogers, M. G. Lagally, R. G. Nuzzo, Nature 2011, 477, 45.
[2] C. C. Striemer, T. R. Gaborski, J. L. McGrath, P. M. Fauchet, Nature 2007, 445, 749.
[3] M. M. Roberts, L. J. Klein, D. E. Savage, K. A. Slinker, M. Friesen, G. Celler, M. A. Eriksson, M. G. Lagally, Nat Mater 2006, 5, 388.
[4] J. Jin, Y. Wakayama, X. Peng, I. Ichinose, Nat Mater 2007, 6, 686.
[5] C. Lee, X. Wei, J. W. Kysar, J. Hone, Science 2008, 321, 385.
[6] K. S. Kim, Y. Zhao, H. Jang, S. Y. Lee, J. M. Kim, K. S. Kim, J. H. Ahn, P. Kim, J. Y. Choi, B. H. Hong, Nature 2009, 457, 706.
[7] E. Kang, J. Ryoo, G. S. Jeong, Y. Y. Choi, S. M. Jeong, J. Ju, S. Chung, S. Takayama, S. H. Lee, Adv Mater 2013, 25, 2167.
[8] H. Watanabe, T. Kunitake, Advanced Materials 2007, 19, 909.
[9] R. Vendamme, S. Y. Onoue, A. Nakao, T. Kunitake, Nat Mater 2006, 5, 494.
[10] C. Jiang, S. Markutsya, Y. Pikus, V. V. Tsukruk, Nat Mater 2004, 3, 721.
[11] S. Markutsya, C. Jiang, Y. Pikus, V. V. Tsukruk, Advanced Functional Materials 2005, 15, 771.
[12] J. H. Kim, A. Nizami, Y. Hwangbo, B. Jang, H. J. Lee, C. S. Woo, S. Hyun, T. S. Kim, Nat Commun 2013, 4, 2520.
[13] K. E. Mueggenburg, X.-M. Lin, R. H. Goldsmith, H. M. Jaeger, Nature materials 2007, 6, 656.
[14] W. Cheng, M. J. Campolongo, J. J. Cha, S. J. Tan, C. C. Umbach, D. A. Muller, D. Luo, Nat Mater 2009, 8, 519.
[15] Y. Chen, Z. Ouyang, M. Gu, W. Cheng, Advanced Materials 2013, 25, 80.
[16] C. Li, D. Cahen, P. Wang, H. Li, J. Zhang, Y. Jin, iScience 2018, 8, 213.
[17] C. Genet, T. W. Ebbesen, Nature 2007, 445, 39.
[18] A. Krishnan, T. Thio, T. J. Kima, H. J. Lezec, T. W. Ebbesen, P. A. Wolff, J. Pendry, L. Martin-Moreno, F. J. Garcia-Vidal, Optics Communications 2001, 200, 1.
[19] A. Dmitriev, C. Hagglund, S. Chen, H. Fredriksson, T. Pakizeh, M. Kall, D. S. Sutherland, Nano Lett 2008, 8, 3893.
[20] M. Najiminaini, F. Vasefi, B. Kaminska, J. J. L. Carson, Appl Phys Lett 2012, 100.
[21] E. S. Kwak, J. Henzie, S. H. Chang, S. K. Gray, G. C. Schatz, T. W. Odom, Nano Lett 2005, 5, 1963.
[22] J. Junesch, T. Sannomiya, Acs Appl Mater Inter 2014, 6, 6322.
[23] S. J. Park, H. Han, H. Rhu, S. Baik, W. Lee, Journal of Materials Chemistry C 2013, 1, 5330.
[24] A. A. Yanik, A. E. Cetin, M. Huang, A. Artar, S. H. Mousavi, A. Khanikaev, J. H. Connor, G. Shvets, H. Altug, Proc Natl Acad Sci U S A 2011, 108, 11784.
[25] S. Kumar, S. Cherukulappurath, T. W. Johnson, S. H. Oh, Chemistry of Materials 2014, 26, 6523.
[26] F. Eftekhari, C. Escobedo, J. Ferreira, X. B. Duan, E. M. Girotto, A. G. Brolo, R. Gordon, D. Sinton, Anal Chem 2009, 81, 4308.
[27] H. Gao, J. Henzie, T. W. Odom, Nano Lett 2006, 6, 2104.
[28] D. D. Galvan, B. Spackova, J. Slaby, F. Sun, Y. H. Ho, J. Homola, Q. M. Yu, J Phys Chem C 2016, 120, 25519.
[29] P. Jia, J. Yang, Opt Express 2015, 23, 18658.

[30] G. P. Collins, Proceedings of the National Academy of Sciences 2016, 113, 240.
[31] W. J. Arora, S. Sijbrandij, L. Stern, J. Notte, H. I. Smith, G. Barbastathis, Journal of Vacuum Science & Technology B: Microelectronics and Nanometer Structures Processing, Measurement, and Phenomena 2007, 25, 2184.
[32] A. Cui, Z. Liu, J. Li, T. H. Shen, X. Xia, Z. Li, Z. Gong, H. Li, B. Wang, J. Li, H. Yang, W. Li, C. Gu, Light: Science & Applications 2015, 4, e308.
[33] K. J. Si, D. Sikdar, Y. Chen, F. Eftekhari, Z. Xu, Y. Tang, W. Xiong, P. Guo, S. Zhang, Y. Lu, Q. Bao, W. Zhu, M. Premaratne, W. Cheng, ACS Nano 2014, 8, 11086.
[34] Y. Mao, Y. Zheng, C. Li, L. Guo, Y. Pan, R. Zhu, J. Xu, W. Zhang, W. Wu, Advanced Materials 2017, 29, 1606482.
[35] W. J. Arora, H. I. Smith, G. Barbastathis, Microelectronic Engineering 2007, 84, 1454.
[36] Z. Liu, H. Du, J. Li, L. Lu, Z. Y. Li, N. X. Fang, Sci Adv 2018, 4, 4436.
[37] M. A. Haque, M. T. A. Saif, P Natl Acad Sci USA 2004, 101, 6335.
[38] A. Carlson, A. M. Bowen, Y. Huang, R. G. Nuzzo, J. A. Rogers, Advanced Materials 2012, 24, 5284.
[39] C. J. Russo, L. A. Passmore, Science 2014, 346, 1377.
[40] A. F. Brilot, J. Z. Chen, A. Cheng, J. Pan, S. C. Harrison, C. S. Potter, B. Carragher, R. Henderson, N. Grigorieff, Journal of Structural Biology 2012, 177, 630.

View Article Online
DOI: 10.1039/C8MH01302K

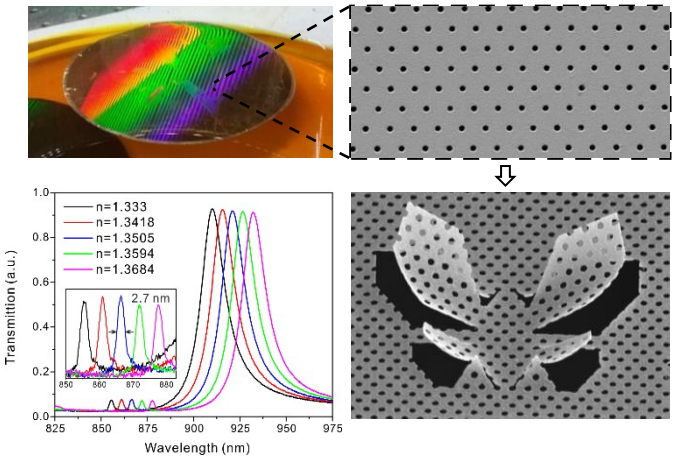

Large-are freestanding gold nanomembranes with nanoholes are created, enabling their property study without substrate effect and emerging applications.